Journal of Biomechanics 84 (2019) 172–182

Contents lists available at ScienceDirect

Journal of Biomechanics

journal homepage: www.elsevier.com/locate/jbiomech
www.JBiomech.com

Is the sheep a suitable model to study the mechanical alterations of disc degeneration in humans? A probabilistic finite element model study

Maxim Bashkuev, Sandra Reitmaier, Hendrik Schmidt *

Charité – Universitätsmedizin Berlin, Corporate Member of Freie Universität Berlin, Humboldt-Universität zu Berlin, and Berlin Institute of Health, Julius Wolff Institute, Germany

ARTICLE INFO

Article history:
Accepted 28 December 2018

Keywords:
Intervertebral disc
Degeneration
Finite element model
Probabilistic
Facet joints

ABSTRACT

Intervertebral disc degeneration is one major source of low back pain, which because of its complex multifactorial nature renders the treatment challenging and thus necessitates extensive research. Experimental animal models have proven valuable in improving our understanding of degenerative processes and potentially promising therapies. Currently, the sheep is the most frequently used large animal *in vivo* model in intervertebral disc research. However, despite its undoubted value for investigations of the complex biological and cellular aspects, to date, it is unclear whether the sheep is also suited to study the mechanical aspects of disc degeneration in *humans*.

A parametric finite element (FE) model of the L4–5 spinal motion segment was developed. Using this model, the geometry and the material properties of both the *human* and the *ovine* spinal segment as well as different appearances of disc degeneration can be depicted. Under pure and combined loads, it was investigated whether degenerative changes to both the *human* and the *ovine* model equivalent caused the same mechanical response.

Different patterns of degeneration resulted in large variations in the ranges of motion, intradiscal pressure, ligament and facet loads. In the *human*, but not in the *ovine* model, all these results differed significantly between different degrees of degeneration.

This FE model study highlighted possible differences in the mechanical response to disc degeneration between *human* and *ovine* intervertebral discs and indicates the necessity of further, more detailed, investigations.

1. Introduction

Low back pain as the leading cause of disability in industrialized countries poses an enormous socio-economic burden with a rising prevalence (Freburger et al., 2009; Martell et al., 2007; Vos et al., 2012; Wolff et al., 2011). The intervertebral disc (IVD) is frequently recognized as the origin of pain (Buckwalter, 1995; Cheung et al., 2009). In particular, the onset of pathologic disc degeneration, characterized by a complex set of morphologic, biochemical, and biologic changes, leads to mechanical dysfunction, and in many cases pain. For many years, *in vivo* animal models have played an important role in the attempt to clarify how degeneration evolves over time either spontaneously or following experimental injury, to determine how constitutive, environmental, or biomechanical risk factors may initiate, promote, or otherwise regulate these changes, and how therapeutic strategies may ameliorate, resolve, or prevent disc degeneration (Lotz, 2004).

A recent review on the use of animal models in IVD research (Reitmaier et al., 2017a) revealed that (1) the most frequently used species between 1985 and 2016 was the sheep, (2) the main focus (73%) of the reported *ovine* studies was the lumbar spine, and (3) 25% of all sheep were utilized to research disc degeneration. However, the representative value of the sheep in investigating the pathomechanisms of *human* disc degeneration as well as to test novel therapeutic interventions is still intensely debated. Similarities in geometrical and material properties as well as disc composition, annulus fiber orientation (Reid et al., 2002), and the absence of notochordal cells (Alini et al., 2008; Osti et al., 1990) are arguments in favor of the sheep model. However, this is contradicted by the significantly smaller disc in sheep, which affects solute diffusion, and considerable interspecies differences in material properties, stature, geometry, and biology (O'Connell et al., 2007; Wang et al., 2015; Wilke et al., 1997b). Furthermore, although the axial orientation of vertebral trabeculae in quadrupeds (Smit, 2002) suggests an axial load direction on the animals' spine comparable to

* Corresponding author at: Julius Wolff Institut, Charité – Universitätsmedizin Berlin, Augustenburger Platz 1, 13353 Berlin, Germany.
E-mail address: hendrik.schmidt@charite.de (H. Schmidt).

https://doi.org/10.1016/j.jbiomech.2018.12.042
0021-9290/

humans, the greater *ovine* vertebral bone mineral density indicates greater compression forces than those in *humans*.

It appears necessary to understand to which extent the *ovine* model is indicative of *human* degenerative conditions. Therefore, the present finite element (FE) model study aimed to investigate how the *human* and the *ovine* motion segments respond to simulated disc degeneration under different loading conditions, while considering natural variations in the geometrical parameters of the spine.

2. Methods

2.1. Parametric FE model

A parametric FE model of a L4–5 spinal motion segment was developed using ANSYS APDL (ANSYS 13.0; ANSYS, Inc., Canonsburg, PA) (Fig. 1a). The model consists of two vertebrae, the intervertebral disc, and seven ligaments; anterior and posterior longitudinal ligaments, intertransverse, interspinous, and supraspinous ligaments, ligamentum flavum, and the capsular ligaments of the facet joints. The vertebrae comprised cortical and cancellous regions, bony endplates, and posterior structures, including pedicles, spinous and transverse processes, and the facet joints. The intervertebral disc incorporated the cartilaginous endplates, the nucleus pulposus, and the annulus fibrosus as a composite of a solid matrix and embedded collagen fibers. Frictionless surface-to-surface contact was assumed between articulating facet surfaces. The facet cartilage layers had a uniform thickness. The model geometry was assumed symmetric along the mid-sagittal plane. By adapting the geometrical parameters, the model allows for the representation of both the *human* and the *ovine* segment (Fig. 1b).

2.2. FE mesh

Eight-node hexahedral fully integrated elements (C3D8) with isotropic linear elastic material properties were used for volumetric structures. The annulus collagen fibers and the ligaments were represented by membrane elements (M3D4) with rebar nonlinear properties. These properties were embedded in the structural elements and did not have any degrees of freedom on their own. The elastic properties of the host elements were negligible and had no influence on the fiber and ligament responses. Twelve criss-cross collagen fiber layers were considered in the radial direction. The fiber angles to the disc mid-height plane varied from ± 30° in the outermost to ± 45° in the innermost layer (Cassidy et al., 1989). Each fiber layer and ligament exhibits nonlinear tension-only relationships (Schmidt et al., 2007, 2006). The material parameters are given in Table 1.

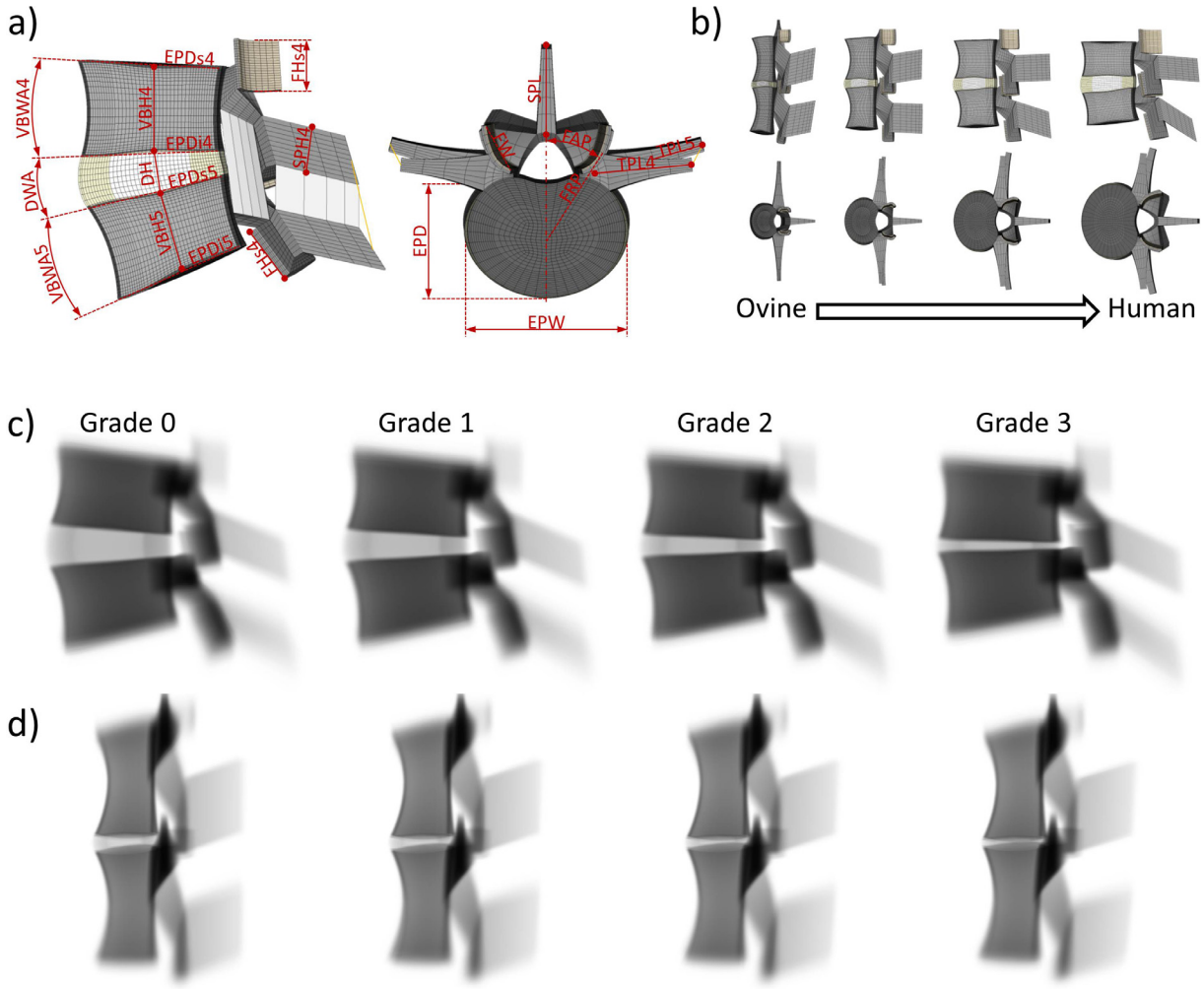

Fig. 1. Parametric finite element model of a human L4–L5 motion segment with main geometrical parameters (a). The parameters are described in Table 2. By setting corresponding parameter values, morphing between human and ovine geometry is possible (b). Simulated "X-rays" (inverted) of the human (c) and ovine (d) models display different stages of degeneration (averaged images of individual models for each grade). Due to averaging, the regions with larger deviations appear blurry.

Table 1
Material properties used in non-degenerated finite element models.

Structure	Material properties	
	Human	*Ovine*
Cortical bone	E = 16000[(1)], ν = 0.3[(2)]	E = 22000[(2)], ν = 0.3[(2)]
Cancellous bone	E = 400, ν = 0.3[(2)]	E = 450, ν = 0.3[(2)]
Posterior elements	E = 400, ν = 0.3[(2)]	E = 500, ν = 0.3[(2)]
Bony endplate	E = 1000, ν = 0.3[(2)]	E = 1000[(3)], ν = 0.3[(2)]
Cartilaginous endplate	E = 100, ν = 0.1	E = 24[(3)], ν = 0.1
Facet cartilage	E = variable, ν = 0.3	E = variable, ν = 0.3
Nucleus pulposus	E = 0.1, ν = variable	E = 0.1, ν = variable
Annulus ground substance	E = variable, ν = 0.2	E = variable, ν = 0.2
Annulus fibers	(Schmidt et al., 2007, 2006)	
Ligaments (anterior longitudinal, posterior longitudinal, flaval, supra- and interspinous, intertransverse and capsular)	(Schmidt et al., 2007)	

E: Young's modulus, ν: Poisson's ratio.
The values are taken from: [(1)](Smit et al., 2002); [(2)](Casaroli et al., 2017); [(3)](Grant et al., 2014); the rest are own values.

2.3. Parameter sampling

Normal distributions of geometrical parameters (Table 2) of the *human* and *ovine* motion segments were assumed. The mean values and standard deviations for both species were taken from the literature (Been et al., 2011; Mageed et al., 2013; O'Connell et al., 2007; Panjabi et al., 1992, 1993; Wilke et al., 1997b). The cross-sectional areas of the annulus fibers were calculated assuming a fiber volumetric fraction of 16% (Galante, 1967). While the nonlinear stress-strain relationships of the ligaments and annulus fibers were considered constant for all models, the cross-sectional areas of the ligaments were varied, based on available literature data for *humans* (Pintar et al., 1992). Because of a lack of data, the *human* values were decreased by 50% for the *ovine* models, approximately proportional to the disc cross-sectional areas. To simulate disc degeneration, the compressibility of the nucleus was assumed to change from 0.0005 mm^2/N in non-degenerated to 0.15 mm^2/N in severely degenerated discs (Rohlmann et al., 2006) while the Young's modulus of the annulus increased. The modeled disc height was calculated by multiplying the non-degenerated value by an additionally uniformly distributed parameter (disc height multiplier) resembling the grading system for degeneration of Mimura et al. (1994).

A custom-made Latin Hypercube Sample (LHS) generator (McKay et al., 1979) was written in Python (Python 2.7, Python Software Foudation), with which the parameter values were calculated by applying the inverse cumulative distribution function to rank transformation of the values from a multivariate normal distribution (Helton and Davis, 2003; Stein, 1987). The positive semi-definite covariance matrix of this distribution was constructed assuming moderate (Pearson's r being in range of 0.5–0.8) pairwise correlations between the parameters of the individual vertebrae (e.g., the width and depth of the L4 endplates were correlated to the width and depth of the L5 endplates, respectively) to avoid unreasonable combinations of geometrical parameters while ensuring sufficient variability in the geometry. Similarly, individual degeneration parameters were assumed correlated (Pearson's r = 0.5) to ensure statistically significant differences between degeneration grades, while allowing for sufficient variability. A sample size of one thousand was generated for both *human* and *ovine* models.

Table 2
Geometrical parameters (units in mm) used to describe the parametric model. The parameters with no standard deviations (SD) are kept constant for all models. The parameters DHM and NUC were converted to uniform distributions by using the corresponding normal cumulative distribution function. DHM determines the actual disc height. Abbreviations are taken from Panjabi et al. (1993, 1992). The SD are reduced due to the nature of LHS sampling covering the complete parameter range.

Parameter	Description	Human (Mean ± SD)	Ovine (Mean ± SD)
VBH4	L4 vertebral body height	24.1 ± 3.81	39.4 ± 1.91
EPWs4	L4 superior endplate width	46.6 ± 4.16	27.4 ± 0.4
EPWi4	L4 inferior endplate width	49.5 ± 4.78	31.0 ± 0.6
EPDs4	L4 superior endplate depth	35.5 ± 3.05	20.8 ± 0.8
EPDi4	L4 inferior endplate depth	33.9 ± 2.94	20.1 ± 0.7
VBWA4	L4 vertebral body wedge angle	2.6 ± 2.8	−6.9 ± 1.4
TPL4	L4 transverse process length	26	38
SPL4	L4 spinous process length	25	20
SPH4	L4 spinous process height	15	25
FWi4	L4 inferior facet width	15	10
FHi4	L4 inferior facet height	15	6
FAPi4	L4 inferior facet angular placement	30	30
FRPi4	L4 inferior facet radial placement	35 ± 0.8	22 ± 0.8
CAXi4	L4 inferior facet card angle CAX	8.8 ± 1.2	10.0 ± 1.2
CAYi4	L4 inferior facet card angle CAY	28 ± 2.0	3.0 ± 0.8
FCT4	L4 facet cartilage thickness	0.6 ± 0.1	0.5 ± 0.1
VBH5	L5 vertebral body height	22.9 ± 3.46	40.6 ± 1.73
EPWs5	L5 superior endplate width	47.3 ± 3.46	28.7 ± 0.42
EPWi5	L5 inferior endplate width	49.4 ± 4.85	32.1 ± 0.62
EPDs5	L5 superior endplate depth	34.7 ± 4.16	20.4 ± 0.79
EPDi5	L5 inferior endplate depth	33.2 ± 3.19	19.5 ± 0.68
VBWA	L5 vertebral body wedge angle	8.4 ± 3.5	−5.1 ± 1.3
TPL5	L5 transverse process length	30	38
SPL5	L5 spinous process length	25	20
SPH5	L5 spinous process height	15	25
FWi5	L5 inferior facet width	15	10
FHi5	L5 inferior facet height	15	6
FAPi5	L5 inferior facet angular placement	33	30
FRPi5	L5 inferior facet radial placement	35 ± 0.8	22 ± 0.8
CAXs5	L5 inferior facet card angle CAX	8.8 ± 1.2	10.0 ± 1.2
CAXs5	L5 inferior facet card angle CAY	28 ± 2.0	3.0 ± 0.8
FCT5	L5 facet cartilage thickness	0.6 ± 0.1	0.5 ± 0.1
DH	Intervertebral disc intact height	11.3 ± 0.3	3.9 ± 0.1
DWA	Intervertebral disc wedge angle	9.8 ± 3.8	4.3 ± 0.15
ALL	ALL cross-sectional area	32.4 ± 2.6	16.2 ± 1.3
PLL	PLL cross-sectional area	5.2 ± 0.35	2.6 ± 0.17
LF	LF cross-sectional area	84.2 ± 5.61	42.1 ± 2.8
ISL	ISL cross-sectional area	35.1 ± 2.34	17.5 ± 1.17
SSL	SSL cross-sectional area	25.2 ± 1.68	12.6 ± 0.84
CL	CL cross-sectional area	43.8 ± 2.92	21.9 ± 1.46
DHM	Disc height multiplier	0.2–1.1	
NUC	Nucleus compressibility	0.0005–0.15	

2.4. Boundary and loading conditions

Five loading scenarios were simulated for each species, resulting in 10,000 simulations in total.

The *human* models were exposed to 1600 N pure axial compression as well as 7.5 Nm flexion and 5.0 Nm extension both with and without an axial compression of 1600 N (Dreischarf et al., 2016a;

Rohlmann et al., 2009a). The *ovine* models were exposed to 320 N pure axial compression as well as 3.75 Nm flexion and 3.75 Nm extension both with and without an axial compression of 320 N (Reitmaier et al., 2014, 2013).

The compressive load was applied as a follower load using a two-node connector element, the nodes of which were rigidly connected to the distal endplates of the corresponding vertebrae by multi-point constraints. The bottom endplate of the lower vertebra was constrained in all degrees of freedom, while flexion and extension moments were applied to the upper node of the connector element.

Mesh refinement was performed under 500 N compressive load followed by 7.5/5 Nm flexion/extension for *human* and 160 N compression followed by 3.75 Nm flexion/extension for *ovine* models until the differences between predicted stress distributions of two consecutive mesh densities fell below 5%. The simulations were performed using the commercial FE software ABAQUS 6.14 (Simulia, Providence, RI, USA).

2.5. Data analysis

For each loading scenario, the ranges of motion (RoM; axial displacement for compression and segmental rotation for flexion/extension, RoF/RoE) were evaluated. Under axial compression, the intradiscal pressure (IDP) was investigated, whereas in flexion, the proportion of the applied flexion moment resisted by the ligaments was calculated as the sum of the individual ligament moments about the center of the nucleus. As in extension most of the ligaments remained unloaded, the axial component of the resulting facet joint forces (including capsular ligaments) was evaluated.

The degree of disc degeneration was determined for each model based on the disc height ratio (ratio of actual disc height to the intact disc height) as follows: non-degenerated (grade 0) = loss of disc height < 20%; mildly degenerated (grade 1) = height loss between 20 and 40%; moderately degenerated (grade 2) = height loss between 40 and 60%; severely degenerated (grade 3) = height loss > 60%. This grading resulted in four equally sized groups (Fig. 1c and d) and the influence of the disc degeneration was statistically evaluated.

2.6. Statistics

The Kolmogorov-Smirnov-Lilliefors test was employed first to test the assumption of normality of each evaluated value. After non-normality of the distributions was found, non-parametric tests were performed for the evaluation. The differences between degeneration grades were investigated using the Kruskal-Wallis-test with Dunn's post-hoc test and Bonferroni correction, and the Wilcoxon signed-rank test was used to evaluate the effect of the preload on the models' response. For pairwise comparisons between matched groups, the 95-percent confidence intervals for the effect size (Cohen's d and Cliff's delta (Rogmann, 2013)) were additionally evaluated for each degeneration grade separately. The effect size was graded as small ($d < 0.5$), medium ($d < 0.8$), and large ($d \geq 0.8$) (Cohen, 1992). The statistical analyses were performed using R 3.2.5 (R Core Team, 2016).

3. Results

3.1. Axial compression

The non-degenerated *human* models (grade 0) predicted a nonlinear load-displacement relationship (Fig. 2a). The extent of

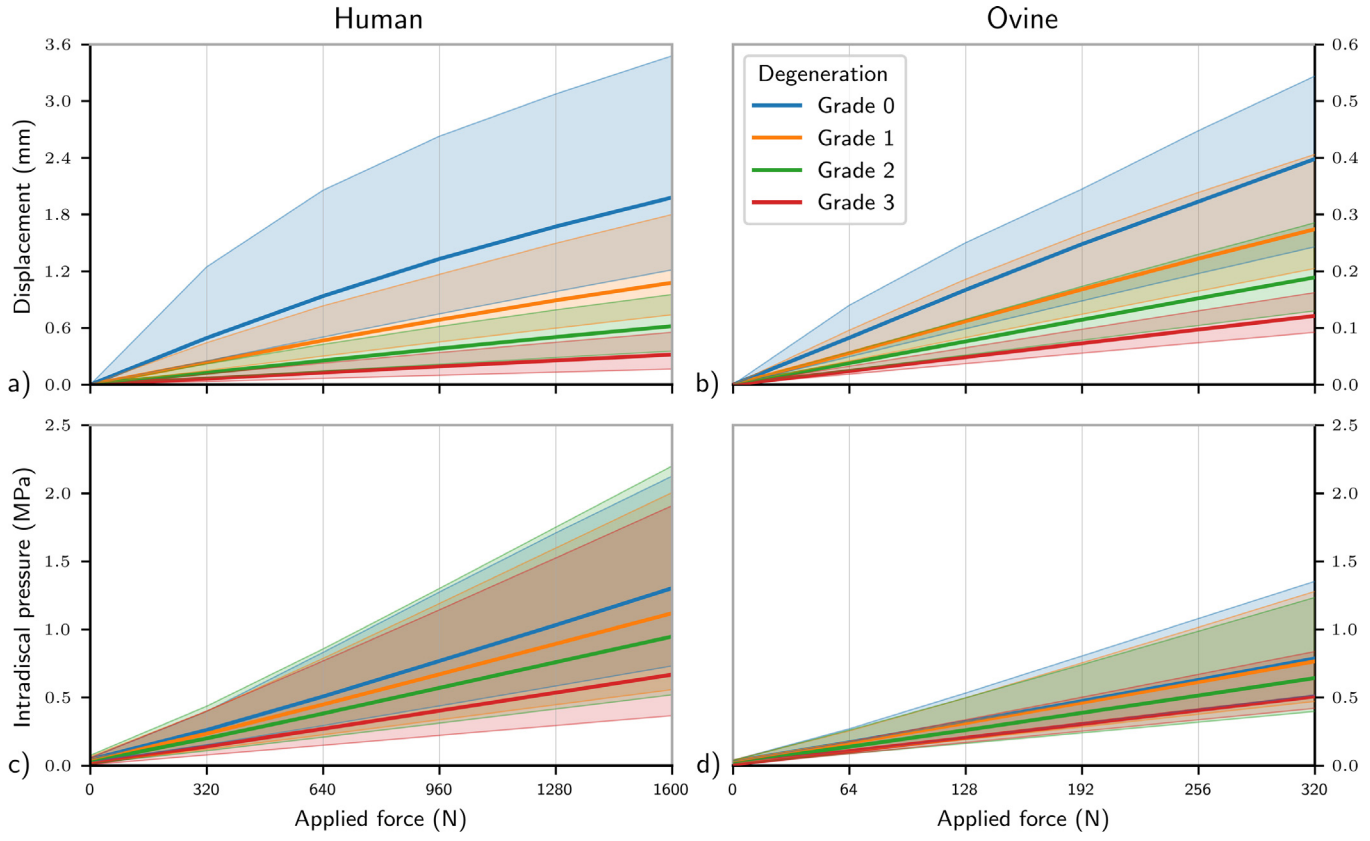

Fig. 2. Median and the interquartile ranges for the response of the motion segments to axial compression grouped by the disc degeneration grade. Human non-degenerated models exhibit a strong nonlinearity of the force-displacement curve (a) in contrast to that of the models affected by degeneration and ovine models (b). Intradiscal pressure increases almost linearly in both species and all degeneration grades (c, d).

nonlinearity varied between individual models and diminished with degeneration. By contrast, the *ovine* models predicted an almost linear load-displacement relationship in all degeneration grades (Fig. 2b).

With progressing degeneration, axial compressive stiffness tended to increase in both species. In *human* models, the median displacement under 1600 N compression was 1.97 mm (range: 1.21–3.48 mm) in the non-degenerated state, and decreased to 1.08 mm (55%), 0.62 mm (31%), and 0.32 mm (16%) in degeneration grades 1, 2, and 3, respectively. In *ovine* models, the median displacement in non-degenerated segments was 0.4 mm and decreased accordingly to 0.27 mm (69%), 0.19 mm (48%), and 0.12 mm (30%) in consecutive increasing degeneration grades.

The IDP displayed an almost linear relationship to the applied load in both *human* (Fig. 2c) and *ovine* (Fig. 2d) models. In both cases, the IDP was greatest in the non-degenerated discs (median: 1.3/0.79 MPa in human/ovine) and decreased with increasing degeneration (1.12/0.77, 0.95/0.64, and 0.67/0.51 MPa in human/ovine at grades 1, 2, and 3, respectively).

3.2. Flexion

Non-degenerated *human* (Fig. 3a) and *ovine* (Fig. 3b) segments displayed a nonlinear behavior ranging over 3.0–6.0° and 3.1–7.9°, respectively. With increasing degeneration, the RoF decreased by 40/29 (Grade 1), 65/48 (Grade 2), and 83/66% (Grade 3) in *human*/*ovine* segments compared to the non-degenerated segments and the motion patterns became more linear in both species. The application of preload increased the RoF in both species; in *human* segments (Fig. 3c) by 40% (Grade 0), 34% (Grade 1), 20% (Grade 2), and 12% (Grade 3) and in *ovine* segments (Fig. 3d) by 3% (Grade 0), 12% (Grade 1), 10% (Grade 2), and 1% (Grade 3).

The median reaction moment resisted by the ligaments increased progressively with the increase of the applied moment in non-degenerated *human* (Fig. 4a) and *ovine* (Fig. 4b) segments. With increasing degeneration, the resistance of ligaments decreased in both species, with the median being almost zero already at grade 1. The maximum values in the individual models decreased exponentially in *human* models (to 3.77, 1.74, and 0.52 Nm at grades 1, 2, and 3, respectively), but almost linearly in *ovine* models (accordingly to 1.74, 0.57, and 0.22 Nm, with increasing grade). The preload significantly decreased the ligament tension in both species (Fig. 4c and d).

3.3. Extension

The predicted median RoE of non-degenerated *human* models was 3.5°, which decreased with progressing degeneration by a mean of 52, 76, and 89% at grades 1, 2, and 3, respectively (Fig. 5a). The *ovine* models predicted a median RoE of 6.0° in non-degenerated segments, which decreased by a mean of 29, 49, and 67% with increasing degeneration (Fig. 5b). Preload reduced the RoE in non-degenerated *human* models to 2.9°, which was further decreased with increasing degeneration by 46, 69, and 85% (Fig. 5c). In *ovine* models, preload reduced the RoE to 5.3° at grade 0. The reduction due to increasing degeneration accounted for 13, 35, and 61% (Fig. 5d). In contrast to *human*, the nonlinear behavior was retained in the *ovine* segments after preload. In both

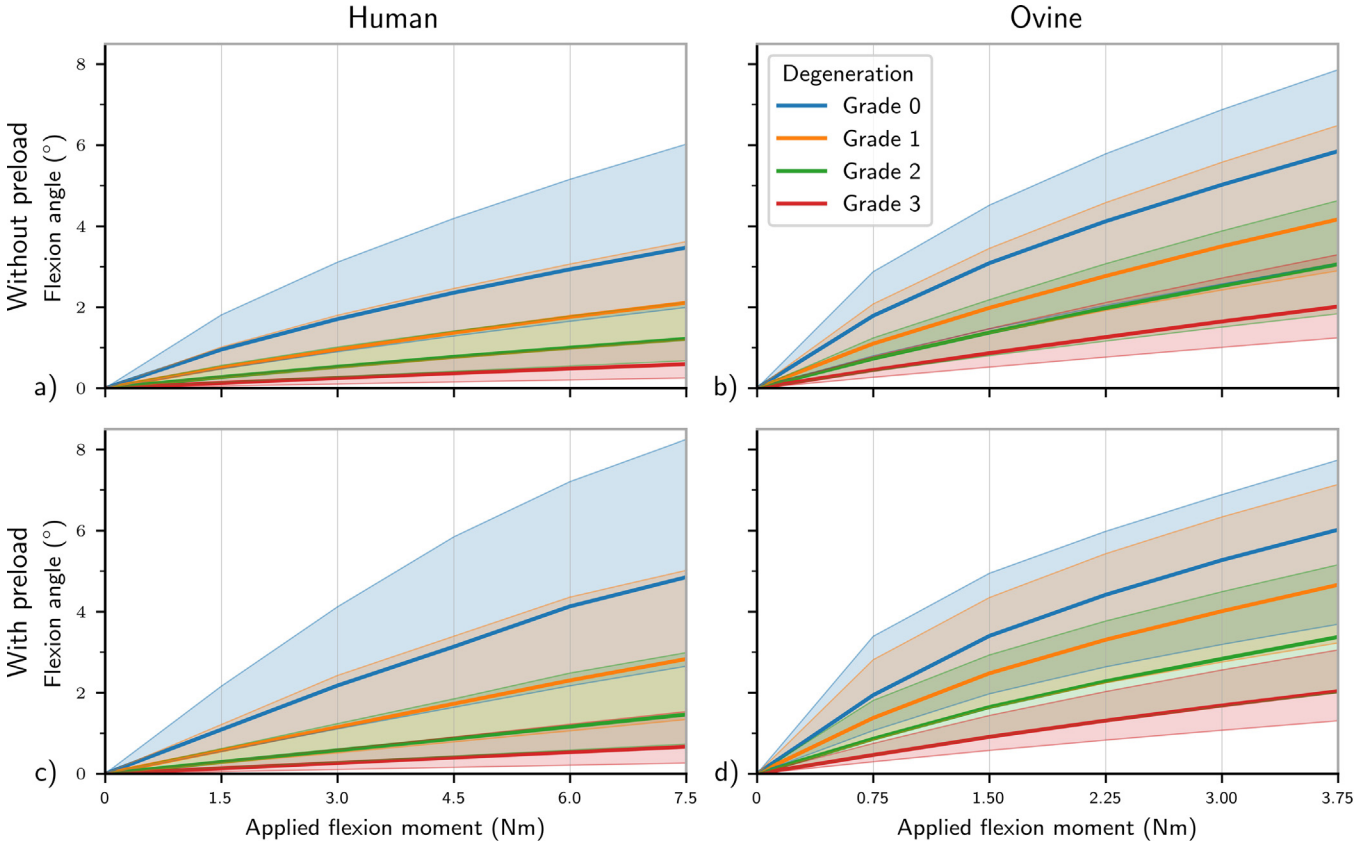

Fig. 3. Median and the interquartile ranges for the response of the human (left) and ovine (right) motion segments to applied flexion moment in pure flexion (top) and after a compressive preload (bottom) grouped by the disc degeneration grade. The bending stiffness of the segments is non-linear and strongly increases with degeneration. Ovine segments display a stronger nonlinearity under low loads both without (b) and with preload (d) as compared to human models (a and c). The human segments become more flexible after preload (c).

species, the ligaments were not active in extension, except for the capsular ligament.

In pure extension, the maximum facet forces reached 50 N in non-degenerated *human* models and 90 N in all degenerated conditions (Fig. 6a). In *ovine* models, to the contrary, the maximum force was largest in non-degenerated models and decreased almost linearly from 108 N to 99, 67, and 47 N at each consecutive degeneration grade (Fig. 6b). The facet force markedly increased with preload in both species (Fig. 6c and d), with corresponding median values at consecutive degeneration grades of 23, 49, 58, and 27 N in *human* and 83, 41, 32, and 7 N in *ovine* models.

3.4. Statistics

None of the investigated values were normally distributed. In compression, the axial displacement in *human* models (Fig. 7a) was significantly different between all degeneration grades ($p < 0.001$, Cohen's $d > 2.8$). The differences in the IDP (Fig. 7b) were small, with $p < 0.001$ and Cohen's $d < 0.3$ for comparisons between adjacent groups. Similarly, for the RoF in *human* models (Fig. 7c), large differences were found between all degeneration grades ($p < 0.001$, Cohen's $d > 2.1$) both under pure flexion and with compressive preload. By contrast, there were no differences in *ovine* models in either loading scenario ($p = 0.75$ and 0.94, respectively). The largest difference in flexion-induced ligament tension (Fig. 7d) was found in pure flexion between degeneration grades 0 and 1 ($p < 0.001$, $d = 2.5$), whereas degeneration grades 2 and 3 showed no significant differences ($p > 0.08$, $d < 0.3$). This difference became significant under compressive preload, but remained small ($p = 0.004$, $d = 0.32$). In extension, the RoM (Fig. 7e) demonstrated the same behavior as in flexion, with large differences in *human* models ($p < 0.001$, $d > 2.1$) and no differences in *ovine* models ($p > 0.74$). In contrast to the ligament tension under flexion, the facet reaction force in extension (Fig. 7f) only displayed negligible differences between groups in pure extension and no differences between degeneration grades 0, 1, and 2 with additional preload. By contrast, *ovine* models predicted no differences between any degeneration grades in all evaluated parameters ($p = 0.33–0.93$).

Paired comparisons revealed a significant effect of preload on all evaluated parameters except for the RoE in *human* models (Table 3), where the preload had no effect under intact and mildly degenerated conditions (grades 0 and 1).

The main difference between species is that in the human but not in the ovine model, the RoM, IDP, ligament, and facet loads differed significantly between different degrees of degeneration.

4. Discussion

Sheep are commonly used as a model for *human* lumbar spinal disc degeneration. The major arguments made to justify the choice of sheep were derived from *in vitro* studies by Wilke et al. (1997a) investigating spinal anatomy. The anatomical study of Wilke et al. (1997b) outlines similarities in "regional trends" between the *ovine* and *human* measurements, but indicated substantial differences in intervertebral disc height (*lumbar* disc heights in sheep are more than 50% smaller than in *humans*). At the same time, the structure of the intervertebral disc and specifically of the annulus fibrosus is similar between the species (Reid et al., 2002). Significant size dif-

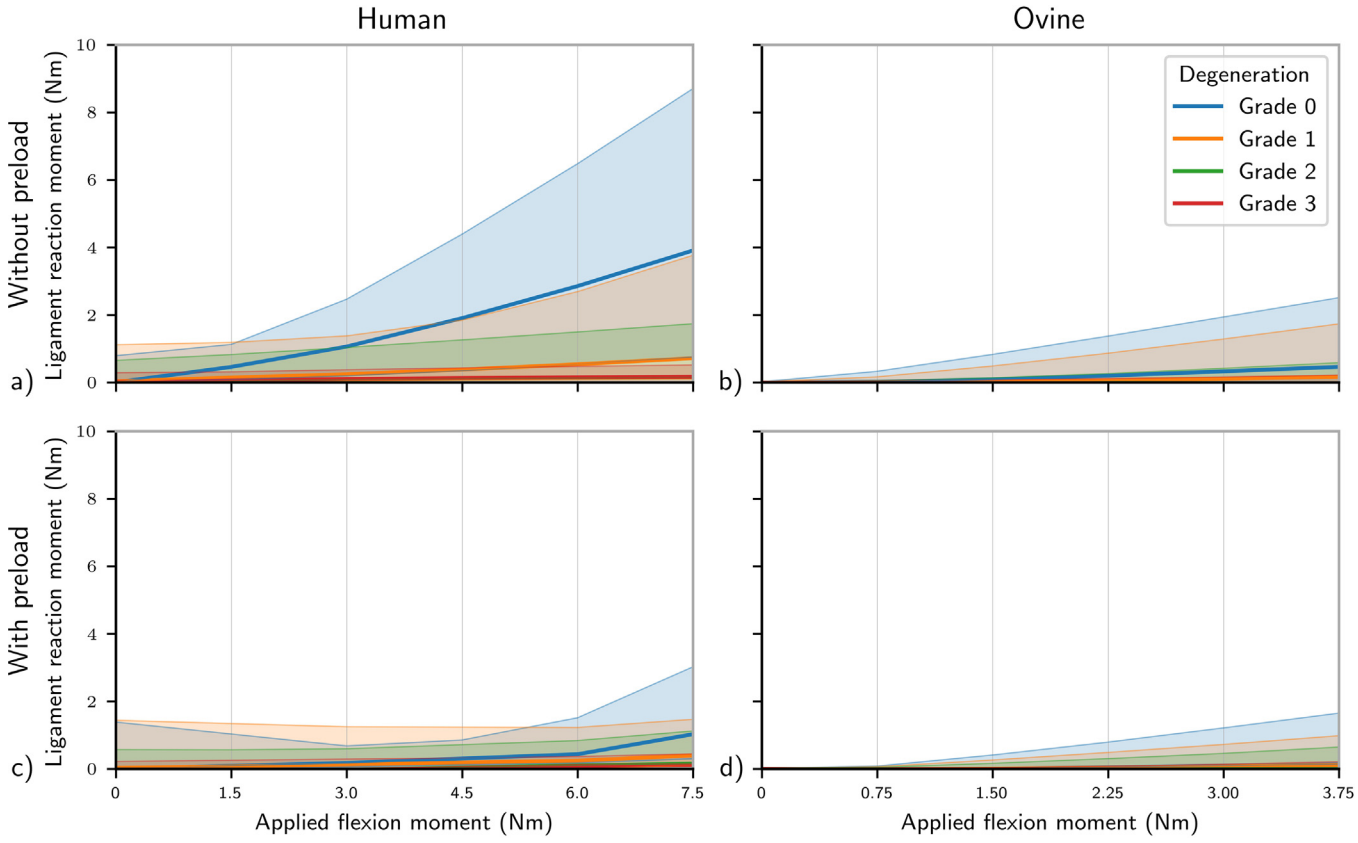

Fig. 4. Median and the interquartile ranges for the reaction moments in the ligaments in response to applied flexion moment in pure flexion (top) and after a compressive preload (bottom) in the human (left) and ovine (right) motion segments. The ligaments in the human non-degenerated models are highly loaded in flexion (a), but this effect rapidly diminishes with increasing degeneration grade. In the ovine models, the ligaments resist a much lower portion of the applied moment and ligament loading increases linearly (b). The preload strongly reduces ligament loading in both human (c) and ovine (d) models.

ferences in the disc play a major role when attempting to extrapolate findings from smaller animal discs to larger *human* discs; for example, under similar diffusion conditions and boundary sources, diffusion pathways are markedly shorter in small discs and hence the solute transport and nutrition of cells are markedly enhanced (Motaghinasab et al., 2014). Valentin and Licka (2016) compared the *in vivo* spinal motion and electromyography (EMG) activity in humans and sheep and raised a note of caution when using sheep as an animal model for spinal research. Preliminary *in vivo* studies measuring the IDP over 24 h in the *lumbar* spine of sheep have also indicated substantial differences between both species (Reitmaier et al., 2013).

The present results suggest that the spinal segments respond to disc degeneration differently in sheep and humans. While the mechanical behavior of *human* models was found to be dependent on the degeneration grade, no significant differences were seen in *ovine* models. Large and almost completely overlapping ranges of the evaluated values and comparable median values at individual degeneration grades made *ovine* models independent of disc degeneration. However, in view of the study limitations, these results should be interpreted carefully.

First, the geometry of the parametric model was simplified, and while the known geometric landmarks (Panjabi et al., 1993, 1992; Wilke et al., 1997b) were considered to allow morphing between human and ovine geometries, these simplifications might influence the model predictions. Second, the most structures were represented using linear elastic materials; viscous effects were neglected. As such, the sources of model nonlinearities are the annulus fibers and the ligaments along with the facet joints. Third, the complex structure of the annulus fibrosus was simplified as concentric layers of continuous fibers embedded into the ground matrix, and the nucleus was assumed as a gel-like substance. While this coarse representation mimics well the mechanical behavior of the intact intervertebral disc, it was not possible to reflect diverse aspects of disc degeneration. As such, the disorganization of the annular fibers in degeneration (Adams, 2012) was not modeled, but this was justified by negligible tension of the annulus fibers. For the same reason, degenerative changes in the individual fibers were also neglected, assuming the elastic properties of the individual fibers and their cross-sectional areas intact in all models. Thus, the disc degeneration was largely modeled as disc height loss combined with change of material properties of the nucleus and the annulus ground substance. A more detailed investigation is necessary to confirm whether or not the neglected aspects of disc degeneration have comparable effects between species. Fourth, osteophyte formation, annular defects such as radial tears and delamination, and endplate calcification were also omitted. It should also be noted that due to the nature of the LHS approach, the design matrix contained model configurations with isolated degenerative changes although in reality they rarely emerge isolated. Last, the exact loads acting in the human and ovine spines are not known, and while the applied loads have been estimated based on published biomechanical studies, they in no case should be considered absolutely correct. Application of different loads could possibly alter the outcome of the simulations.

An 800 N compression was assumed for the *human* models simulating standing. While 500 N axial compression is frequently suggested for standing (e.g., Rohlmann et al., 2009b; Sato et al., 1999), the range of loads found in the literature is quite large, sometimes exceeding 1000 N at the L4–L5 spinal level (Dreischarf et al.,

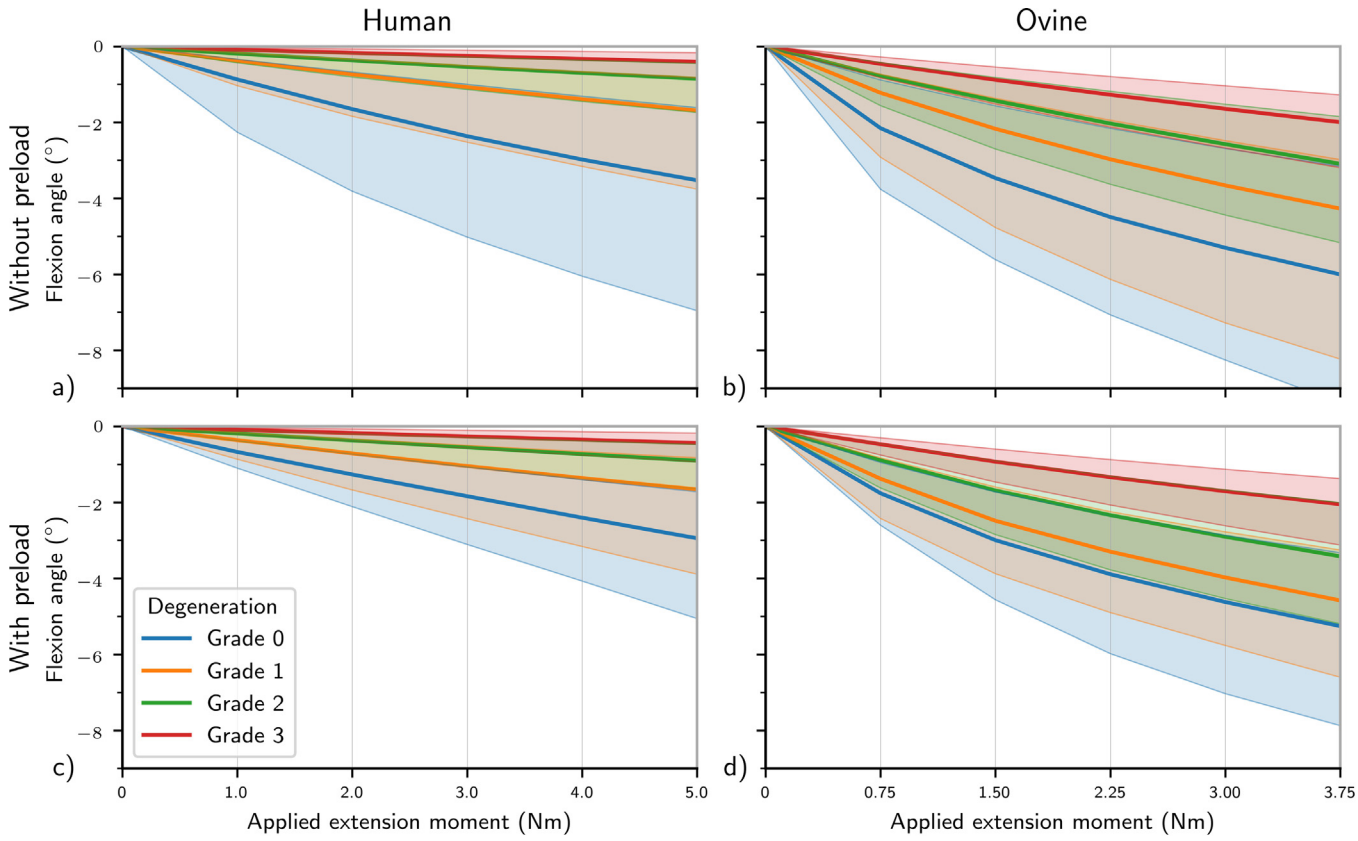

Fig. 5. Median and the interquartile ranges for the response of the human (left) and ovine (right) motion segments to applied extension moment in pure flexion (top) and after a compressive preload (bottom). The bending stiffness of all segments is non-linear and strongly increases with degeneration. The nonlinearity diminishes with increasing degeneration in both human (a) and ovine (b) segments. After compressive preload, the response becomes fairly linear in human (c), but not in ovine segments (d). Both species demonstrate an increase in stiffness after preload.

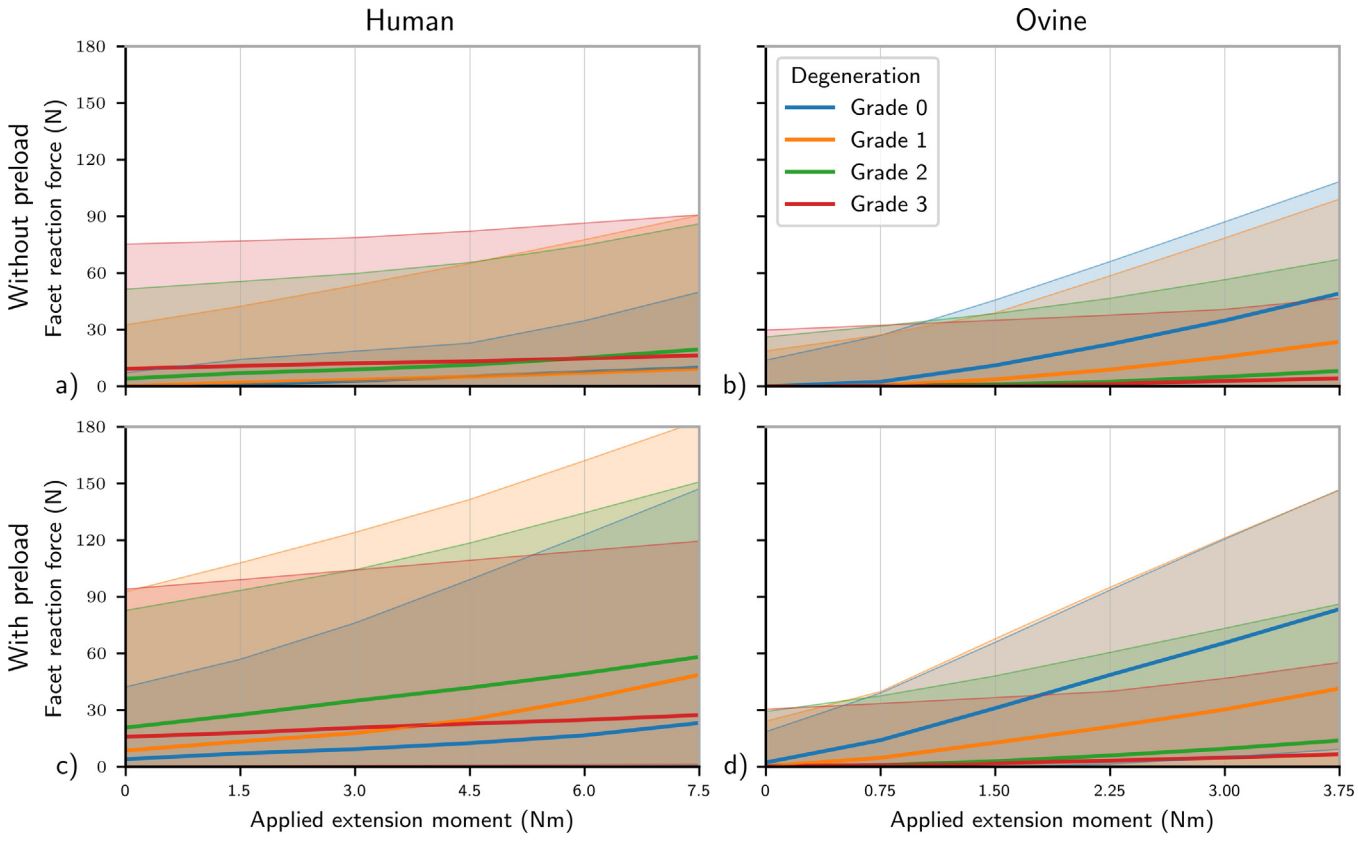

Fig. 6. Median and the interquartile ranges for the facet reaction forces in response to applied extension moment without (top) and with compressive preload (bottom) in the human (left) and ovine (right) segments. The facet ligament forces in the human non-degenerated models were highly loaded in flexion (a), but this effect rapidly diminishes with increasing degeneration grade. In the ovine models, the ligaments resist a much lower portion of the applied moment and ligament loading increases linearly (b). The preload strongly reduces ligament loading in both human (c) and ovine (d) models.

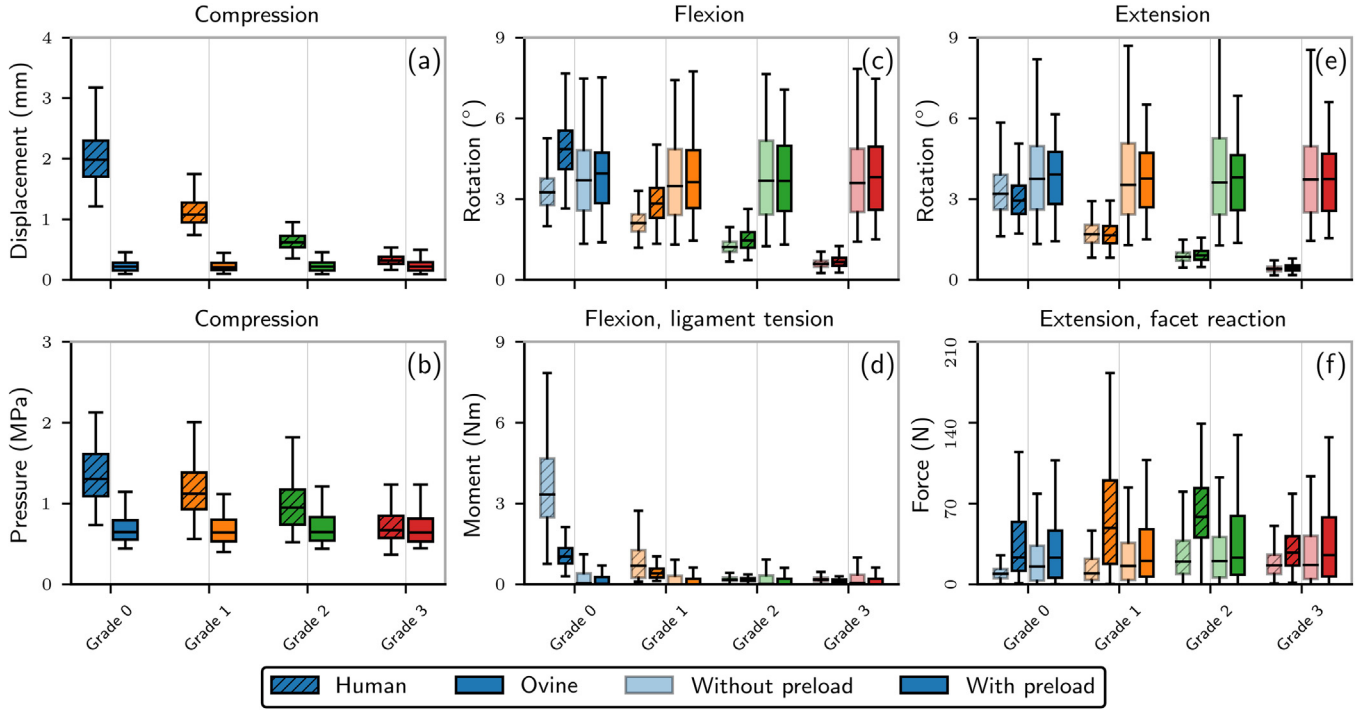

Fig. 7. Boxplots of the statistically evaluated values. Significant differences were found in all variables between different degeneration grades as well as between loading conditions (with and without preload) in human models. No differences were found in ovine models.

Table 3
P-values and corresponding 95% confidence intervals (CI) for the effect-size estimates (Cohen's delta and Cliff's delta) for the paired comparisons showing the effect of preload. RoM: Range of Motion.

Parameter			Grade	p-value	Cohen's d	95% CI	Cliff's d	95% CI
Flexion	*Human*	RoM	0	<0.001	3.16	2.83–3.50	1.85	1.90–1.80
			1	<0.001	2.06	1.83–2.28	1.59	1.64–1.54
			2	<0.001	1.61	1.40–1.82	1.36	1.39–1.32
			3	<0.001	1.31	1.11–1.51	1.17	1.21–1.13
		Ligament moment	0	<0.001	4.22	3.82–4.62	2.00	2.00–2.00
			1	<0.001	3.78	3.48–4.08	2.00	2.00–2.00
			2	<0.001	3.06	2.80–3.33	2.00	2.00–2.00
			3	<0.001	3.00	2.74–3.26	2.00	2.00–2.00
	Ovine	RoM	0	<0.001	1.56	1.25–1.86	1.19	1.15–1.24
			1	<0.001	1.44	1.19–1.69	1.16	1.14–1.18
			2	<0.001	1.49	1.23–1.76	1.16	1.14–1.19
			3	<0.001	1.44	1.19–1.68	1.17	1.14–1.20
		Ligament moment	0	<0.001	1.24	0.95–1.53	0.98	0.59–1.00
			1	<0.001	0.89	0.66–1.13	0.91	0.77–0.97
			2	<0.001	0.79	0.55–1.04	0.90	0.74–0.96
			3	<0.001	1.02	0.78–1.26	0.93	0.78–0.98
Extension	*Human*	RoM	0	0.003	0.15	−0.08–0.39	0.49	0.25–0.67
			1	0.21	0.00	−0.18–0.18	0.09	−0.06–0.24
			2	<0.001	0.86	0.68–1.05	0.85	0.73–0.92
			3	<0.001	1.99	1.77–2.21	1.12	1.11–1.14
		Facet reaction force	0	<0.001	4.49	4.05–4.94	2.00	2.00–2.00
			1	<0.001	3.82	3.52–4.12	2.00	2.00–2.00
			2	<0.001	3.06	2.80–3.33	2.00	2.00–2.00
			3	<0.001	2.98	2.72–3.24	2.00	2.00–2.00
	Ovine	RoM	0	<0.001	1.80	1.48–2.12	1.12	1.07–1.23
			1	<0.001	1.92	1.65–2.19	1.16	1.14–1.18
			2	<0.001	1.85	1.57–2.13	1.14	1.11–1.19
			3	<0.001	1.74	1.48–2.00	1.12	1.07–1.18
		Facet reaction force	0	<0.001	0.97	0.68–1.25	1.18	1.16–1.20
			1	<0.001	0.96	0.72–1.19	1.18	1.16–1.20
			2	<0.001	1.06	0.80–1.31	1.19	1.16–1.21
			3	<0.001	1.02	0.78–1.25	1.15	1.10–1.22

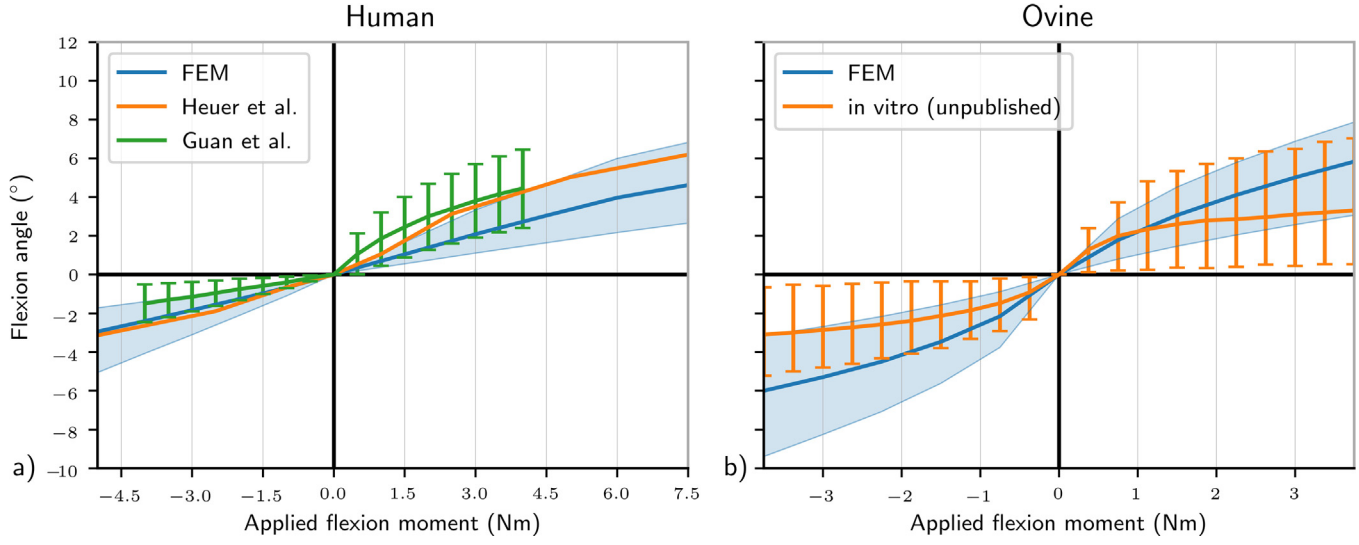

Fig. 8. Comparison between model predictions and experimental data under flexion/extension moments. While human models (a) were compared to the published literature data (Guan et al., 2007; Heuer et al., 2007), the ovine models (b) were compared to the data acquired during in-house in vitro experiments.

2016b). In *ovine* models, a compressive load of 160 N was assumed (Hauerstock et al., 2001; Reitmaier et al., 2013). Since the spinal loads are known to drastically increase in dynamic activities and have been measured to be a two-fold of the body weight in level walking (Rohlmann et al., 2008), the assumed values were doubled reaching 1600 and 320 N compression, respectively. Because of different load magnitudes, the resulting RoMs and forces cannot be directly compared between *human* and *ovine* models; however, because the changes in the segment mechanics in response to degeneration were of interest, a one-to-one comparison of the predicted values between the species is not necessary.

Since most of the published axial compression test data depend on the load application rate, an exact one-to-one comparison of the predicted results was considered meaningless. Validating the intact models based on the intradiscal pressure predictions was also not possible since the osmotic pressure was not modeled. In extension, the human models predictions were in an excellent agreement to the experimental results of Heuer et al. (2007), while

Guan et al. (2007) reported a stiffer and nearly linear behavior. In flexion, both datasets indicated a more compliant behavior than predicted by the models (Fig. 8). However, Wang et al. (2014) tested six L4-L5 human specimens under pure moments of 8 Nm and found the average range of flexion of 4.3°, which is comparable to that of the presented models (4.6°). Taking into account the large variations of the reported experimental findings, the model predictions were considered reasonable. While the ovine models exhibited more compliant behavior compared to the in-house experimental data from intact ovine specimens (partially published by Reitmaier et al. (2017b, 2014)), the predicted ranges overlap to a large extent with the experimental data.

The predicted non-linear force–displacement response of human models to compressive or bending loads is in agreement with previous *in vitro* (Berkson et al., 1979; Markolf, 1972; Tencer et al., 1982) and computational model studies (Shirazi-Adl et al., 1986). With increasing degeneration, the displacement response linearizes because of the negligible mechanical role of collagen fibers under smaller disc heights and higher nucleus compressibility. The predicted gradual reduction of the RoM with degeneration agrees well with *in vitro* observations (Mimura et al., 1994; Zirbel et al., 2013). While a decreased stiffness has also been observed in mildly degenerated specimens (Fujiwara et al., 2000, 1999; Kirkaldy-Willis and Farfan, 1982), individual tissues exhibit significant stiffening with degeneration (Wang et al., 2012), which gives the reason to consider the predicted behavior plausible.

In contrast to *human* models, the smaller initial disc height and the greater endplate curvature of *ovine* models resulted in smaller disc bulges in compression and thus in a more linear response due to a lower involvement of collagen fibers. By contrast, the smaller cross-sectional area in *ovine* models caused a greater contribution of fibers in flexion and extension. *Ovine* models displayed a negligible effect of degeneration on the model response to applied loads, which is in contrast to previous *in vitro* and *in vivo* findings that demonstrated a significant, although greatly debated, change in segmental stiffness following degeneration.

As indicated previously, the differences in posture cast serious doubts on the credibility of the *ovine* model for spinal research in humans. In quadrupeds, the spine is likely exposed to high bending moments as opposed to humans. However, these are balanced by the muscles and ligaments (Smit, 2002). At the same time, because of their orientation and shape, the facet joints of the lumbar region constrain the axial rotation and extension (Cotterill et al., 1986), effectively protecting the IVD from rotational stresses (Farfan and Sullivan, 1967; Sullivan et al., 1971). Therefore, the main loading of the spine remains the axial compression in quadrupeds. In the present simulations, differences in the geometry of facet joints led to different shares of the load transmitted through the disc and the facet joints in human and sheep: while the loads transmitted through the facet joints in extension did not display any clear pattern in human, the facet loads increased linearly with the magnitude of the applied moment and grew further under preload in *ovine* models, and demonstrated a decreasing tendency with progressing degeneration.

In conclusion, while this FE model study highlighted possible differences in the mechanical response to disc degeneration between human and ovine intervertebral discs, the results should be considered carefully in view of the model limitations. However, the fact that a rather limited representation of the disc degeneration predicted such differences indicates that more efforts have to be put into more detailed investigations in the future work, including, but not limited to a more detailed modeling of the disc structure and degeneration induced structural changes.

Conflict of interest

None of the authors has any conflicts of interests to declare.

Acknowledgments

This study was financially supported by the German Research Foundation (DFG), SCHM 2572/4-1; SCHM 2772/6-1.

References

Adams, M.A., 2012. Basic science of spinal degeneration. Surg. (U. K.) 30, 347–350. https://doi.org/10.1016/j.mpsur.2012.05.003.
Alini, M., Eisenstein, S.M., Ito, K., et al., 2008. Are animal models useful for studying human disc disorders/degeneration? Eur. Spine J. 17, 2–19. https://doi.org/10.1007/s00586-007-0414-y.
Been, E., Li, L., Hunter, D.J., Kalichman, L., 2011. Geometry of the vertebral bodies and the intervertebral discs in lumbar segments adjacent to spondylolysis and spondylolisthesis: pilot study. Eur. Spine J. 20, 1159–1165. https://doi.org/10.1007/s00586-010-1660-y.
Berkson, M.H., Nachemson, A., Schultz, A.B., 1979. Mechanical properties of human lumbar spine motion segments - Part II: responses in compression and shear; influence of gross morphology. J. Biomech. Eng. 101, 53–57. https://doi.org/10.1115/1.3426225.
Buckwalter, J.A., 1995. Aging and degeneration of the human intervertebral disc. Spine(Phila. Pa. 1976) 20, 1307–1314.
Cassidy, J.J., Hiltner, A., Baer, E., 1989. Hierarchical structure of the intervertebral disc. Connect. Tissue Res. 23, 75–88.
Casaroli, G., Galbusera, F., Jonas, R., Schlager, B., Wilke, H.J., Villa, T., 2017. A novel finite element model of the ovine lumbar intervertebral disc with anisotropic hyperelastic material properties. PLoS ONE 12(5), 1–18. https://doi.org/10.1371/journal.pone.0177088.
Cheung, K.M.C., Karppinen, J., Chan, D., et al., 2009. Prevalence and pattern of lumbar magnetic resonance imaging changes in a population study of one thousand forty-three individuals. Spine (Phila Pa 1976) 34, 934–940. https://doi.org/10.1097/BRS.0b013e3181a01b3f.
Cohen, J., 1992. A power primer. Psychol. Bull. 112, 155–159. https://doi.org/10.1037/0033-2909.112.1.155.
Cotterill, P.C., Kostuik, J.P., D'Angelo, G., et al., 1986. An anatomical comparison of the human and bovine thoracolumbar spine. J. Orthop. Res. 4, 298–303. https://doi.org/10.1002/jor.1100040306.
Dreischarf, M., Rohlmann, A., Graichen, F., et al., 2016a. In vivo loads on a vertebral body replacement during different lifting techniques. J. Biomech. 49, 890–895. https://doi.org/10.1016/j.jbiomech.2015.09.034.
Dreischarf, M., Shirazi-Adl, A., Arjmand, N., et al., 2016b. Estimation of loads on human lumbar spine: a review of in vivo and computational model studies. J. Biomech. 49, 833–845. https://doi.org/10.1016/j.jbiomech.2015.12.038.
Farfan, H.F., Sullivan, J.D., 1967. The relation of facet orientation to intervertebral disc failure. Can. J. Surg. 10, 179–185.
Freburger, J., Holmes, G., Agans, R., et al., 2009. The rising prevalence of chronic low back pain. Arch. Intern. Med. 169, 251–258. https://doi.org/10.1001/archinternmed.2008.543.
Fujiwara, A., Tamai, K., An, H.S., et al., 2000. The relationship between disc degeneration, facet joint osteoarthritis, and stability of the degenerative lumbar spine. J. Spinal Disord. 13, 444–450. https://doi.org/10.1097/00002517-200010000-00013.
Fujiwara, A., Tamai, K., Yamato, M., et al., 1999. The relationship between facet joint osteoarthritis and disc degeneration of the lumbar spine: an MRI study. Eur. Spine J. 8, 396–401 https://doi.org/90080396.586.
Galante, J.O., 1967. Tensile properties of the human lumbar annulus fibrosus. Acta Orthop. Scand. 38, 1–91. https://doi.org/10.3109/ort.1967.38.suppl-100.01.
Grant, C.A., Wilson, L.J., Langton, C., Epari, D., 2014. Comparison of mechanical and ultrasound elastic modulus of ovine tibial cortical bone. Med. Eng. Phy. 36(7), 869–874. https://doi.org/10.1016/j.medengphy.2014.03.012.
Guan, Y., Yoganandan, N., Moore, J., et al., 2007. Moment-rotation responses of the human lumbosacral spinal column. J. Biomech. 40, 1975–1980. https://doi.org/10.1016/j.jbiomech.2006.09.027.
Hauerstock, D., Reindl, R., Steffen, T., 2001. Telemetric measurement of compressive loads in the sheep lumbar spine. Transactions of the 47th Annual Meeting of The Orthopaedic Research Society. San Francisco, California.
Helton, J.C., Davis, F.J., 2003. Latin hypercube sampling and the propagation of uncertainty in analyses of complex systems. Reliab. Eng. Syst. Saf. 81, 23–69. https://doi.org/10.1016/S0951-8320(03)00058-9.
Heuer, F., Schmidt, H., Claes, L., Wilke, H.J., 2007. Stepwise reduction of functional spinal structures increase vertebral translation and intradiscal pressure. J. Biomech. 40, 795–803. https://doi.org/10.1016/j.jbiomech.2006.03.016.
Kirkaldy-Willis, W.H., Farfan, H.F., 1982. Instability of the lumbar spine. Clin. Orthop. Relat. Res. 10, 110–123.
Lotz, J.C., 2004. Animal models of intervertebral disc degeneration: lessons learned. Spine (Phila. Pa. 1976) 29, 2742–2750. https://doi.org/10.1097/01.brs.0000146498.04628.f9.

Mageed, M., Berner, D., Jülke, H., et al., 2013. Is sheep lumbar spine a suitable alternative model for human spinal researches? Morphometrical comparison study. Lab. Anim. Res. 29, 183–189. https://doi.org/10.5625/lar.2013.29.4.183.

Markolf, K.L., 1972. Deformation of the thoracolumbar intervertebral joints in response to external loads: a biomechanical study using autopsy material. J. Bone Joint Surg. Am. 54, 511–533.

Martell, B.A., O'Connor, P.G., Kerns, R.D., et al., 2007. Systematic review: opioid treatment for chronic back pain: prevalence, efficacy, and association with addiction. Ann. Intern. Med. 146, 116–127.

McKay, M.D., Beckman, R.J., Conover, W.J., 1979. A comparison of three methods for selecting values of input variables in the analysis of output from a computer code. Technometrics 21, 239. https://doi.org/10.2307/1268522.

Mimura, M., Panjabi, M.M., Oxland, T.R., et al., 1994. Disc degeneration affects the multidirectional flexibility of the lumbar spine. Spine (Phila. Pa. 1976). https://doi.org/10.1097/00007632-199406000-00011.

Motaghinasab, S., Shirazi-Adl, A., Parnianpour, M., Urban, J.P.G., 2014. Disc size markedly influences concentration profiles of intravenously administered solutes in the intervertebral disc: a computational study on glucosamine as a model solute. Eur. Spine J. 23, 715–723. https://doi.org/10.1007/s00586-013-3142-5.

O'Connell, G.D., Vresilovic, E.J., Elliott, D.M., 2007. Comparison of animals used in disc research to human lumbar disc geometry. Spine (Phila. Pa. 1976) 32, 328–333. https://doi.org/10.1097/01.brs.0000253961.40910.c1.

Osti, O.L., Vernon-Roberts, B., Fraser, R.D., 1990. Volvo Award in experimental studies. Anulus tears and intervertebral disc degeneration. An experimental study using an animal model. Spine. <https://doi.org/10.1097/00007632-199008010-00005>

Panjabi, M.M., Goel, V., Oxland, T., 1992. Human lumbar vertebrae: quantitative three-dimensional anatomy. Spine (Phila. Pa. 1976) 17, 299–306.

Panjabi, M.M., Oxland, T., Takata, K., et al., 1993. Articular facets of the human spine. Quantitative three-dimensional anatomy. Spine (Phila. Pa. 1976) 18, 1298–1310. https://doi.org/10.1097/00007632-199308000-00009.

Pintar, F.A., Yoganandan, N., Myers, T., et al., 1992. Biomechanical properties of human lumbar spine ligaments. J. Biomech. 25, 1351–1356.

R Core Team, 2016. R: A Language and Environment for Statistical Computing [WWW Document]. URL <https://www.r-project.org/>

Reid, J.E., Meakin, J.R., Robins, S.P., et al., 2002. Sheep lumbar intervertebral discs as models for human discs. Clin. Biomech. 17, 312–314. https://doi.org/10.1016/S0268-0033(02)00009-8.

Reitmaier, S., Graichen, F., Shirazi-Adl, A., Schmidt, H., 2017a. Separate the sheep from the goats. J. Bone Jt. Surg. 99, e102. https://doi.org/10.2106/JBJS.17.00172.

Reitmaier, S., Schmidt, H., Ihler, R., et al., 2013. Preliminary investigations on intradiscal pressures during daily activities: an in vivo study using the merino sheep. PLoS One 8, e69610. https://doi.org/10.1371/journal.pone.0069610.

Reitmaier, S., Schuelke, J., Schmidt, H., et al., 2017b. Spinal fusion without instrumentation – experimental animal study. Clin. Biomech. 46, 6–14. https://doi.org/10.1016/j.clinbiomech.2017.04.008.

Reitmaier, S., Volkheimer, D., Berger-Roscher, N., et al., 2014. Increase or decrease in stability after nucleotomy? Conflicting in vitro and in vivo results in the sheep model 20140650–20140650 J. R. Soc. Interface 11. https://doi.org/10.1098/rsif.2014.0650.

Rogmann, J.J., 2013. Ordinal Dominance Statistitcs (orddom): An R Project for Statistical Computing package to compute ordinal, nonparametric alternatives to mean comparisons. Available from: <https://cran.r-project.org/package=orddom>.

Rohlmann, A., Graichen, F., Bender, A., et al., 2008. Loads on a telemeterized vertebral body replacement measured in three patients within the first postoperative month. Clin. Biomech. (Bristol, Avon) 23, 147–158. https://doi.org/10.1016/j.clinbiomech.2007.09.011.

Rohlmann, A., Zander, T., Rao, M., Bergmann, G., 2009a. Realistic loading conditions for upper body bending. J. Biomech. 42, 884–890. https://doi.org/10.1016/j.jbiomech.2009.01.017.

Rohlmann, A., Zander, T., Rao, M., Bergmann, G., 2009b. Applying a follower load delivers realistic results for simulating standing. J. Biomech. 42, 1520–1526. https://doi.org/10.1016/j.jbiomech.2009.03.048.

Rohlmann, A., Zander, T., Schmidt, H., et al., 2006. Analysis of the influence of disc degeneration on the mechanical behaviour of a lumbar motion segment using the finite element method. J. Biomech. 39, 2484–2490. https://doi.org/10.1016/j.jbiomech.2005.07.026.

Sato, K., Kikuchi, S., Yonezawa, T., 1999. In vivo intradiscal pressure measurement in healthy individuals and in patients with ongoing back problems. Spine (Phila. Pa. 1976) 24, 2468–2474. https://doi.org/10.1097/00007632-199912010-00008.

Schmidt, H., Heuer, F., Drumm, J., et al., 2007. Application of a calibration method provides more realistic results for a finite element model of a lumbar spinal segment. Clin. Biomech. 22, 377–384. https://doi.org/10.1016/j.clinbiomech.2006.11.008.

Schmidt, H., Heuer, F., Simon, U., et al., 2006. Application of a new calibration method for a three-dimensional finite element model of a human lumbar annulus fibrosus. Clin. Biomech. 21, 337–344. https://doi.org/10.1016/j.clinbiomech.2005.12.001.

Shirazi-Adl, A., Ahmed, A.M., Shrivastava, S.C., 1986. A finite element study of a lumbar motion segment subjected to pure sagittal plane moments. J. Biomech. 19, 331–350.

Smit, T.H., 2002. The use of a quadruped as an in vivo model for the study of the spine - biomechanical considerations. Eur. Spine J. 11, 137–144. https://doi.org/10.1007/s005860100346.

Stein, M., 1987. Large sample properties of simulations using latin hypercube sampling. Technometrics 29, 143–151. https://doi.org/10.1080/00401706.1987.10488205.

Sullivan, J.D., Farfan, H.F., Kahn, D.S., 1971. Pathologic changes with intervertebral joint rotational instability in the rabbit. Can. J. Surg. 14, 71–79.

Tencer, A.F., Ahmed, A.M., Burke, D.L., 1982. Some static mechanical properties of the lumbar intervertebral joint, intact and injured. J. Biomech. Eng. 104, 193–201. https://doi.org/10.1115/1.3138348.

Valentin, S., Licka, T.F., 2016. Spinal motion and muscle activity during active trunk movements - comparing sheep and humans adopting upright and quadrupedal postures. PLoS One 11, 1–16. https://doi.org/10.1371/journal.pone.0146362.

Vos, T., Flaxman, A.D., Naghavi, M., et al., 2012. Years lived with disability (YLDs) for 1160 sequelae of 289 diseases and injuries 1990–2010: a systematic analysis for the Global Burden of Disease Study 2010. Lancet 380, 2163–2196. https://doi.org/10.1016/S0140-6736(12)61729-2.

Wang, X., Xu, J., Zhu, Y., et al., 2014. Biomechanical analysis of a newly developed shape memory alloy hook in a transforaminal lumbar interbody fusion (TLIF) in vitro model. PLoS One 9, e114326. https://doi.org/10.1371/journal.pone.0114326.

Wang, Y., Chen, H.-B., Zhang, L., et al., 2012. Influence of degenerative changes of intervertebral disc on its material properties and pathology. Chinese J. Traumatol. 15, 67–76. https://doi.org/10.3760/cma.j.issn.1008-1275.2012.02.001.

Wang, Y., Liu, T., Song, L.-S., et al., 2015. Anatomical characteristics of deer and sheep lumbar spines: comparison to the human lumbar spine. Int. J. Morphol. 33, 105–112.

Wilke, H.-J., Kettler, A., Claes, L.E., 1997a. Are sheep spines a valid biomechanical model for human spines? Spine (Phila. Pa. 1976) 22, 2365–2374. https://doi.org/10.1097/00007632-199710150-00009.

Wilke, H.-J., Kettler, A., Wenger, K.H., Claes, L.E., 1997b. Anatomy of the sheep spine and its comparison to the human spine. Anat. Rec. 247, 542–555. https://doi.org/10.1002/(SICI)1097-0185(199704)247:4<542::AID-AR13>3.0.CO;2-P.

Wolff, R., Clar, C., Lerch, C., Kleijnen, J., 2011. Epidemiology of chronic non-malignant pain in Germany. Schmerz 25, 26–44. https://doi.org/10.1007/s00482-010-1011-2.

Zirbel, S.A., Stolworthy, D.K., Howell, L.L., Bowden, A.E., 2013. Intervertebral disc degeneration alters lumbar spine segmental stiffness in all modes of loading under a compressive follower load. Spine J. 13, 1134–1147. https://doi.org/10.1016/j.spinee.2013.02.010.